Inorganic Chemistry

Article

pubs.acs.org/IC

Imino–Phenolic–Pyridyl Conjugates of Calix[4]arene (L_1 and L_2) as Primary Fluorescence *Switch-on* Sensors for Zn^{2+} in Solution and in HeLa Cells and the Recognition of Pyrophosphate and ATP by [ZnL_2]

Rakesh Kumar Pathak,[†] Vijaya Kumar Hinge,[‡] Ankit Rai,[‡] Dulal Panda,[‡] and Chebrolu Pulla Rao*[,†,‡]

[†]Bioinorganic Laboratory & Department of Chemistry and [‡]Department of Biosciences & Bioengineering, Indian Institute of Technology Bombay, Powai, Mumbai 400 076, India

Supporting Information

ABSTRACT: Pyridyl-based triazole-linked calix[4]arene conjugates, viz. $\mathbf{L_1}$ and $\mathbf{L_2}$, were synthesized and characterized. These two conjugates were shown to be selective and sensitive for Zn^{2+} among the 12 metal ions studied in HEPES buffer medium by fluorescence, absorption, and visual color change with the detection limit of ~31 and ~112 ppb, respectively, by $\mathbf{L_1}$ and $\mathbf{L_2}$. Moreover, the utility of the conjugates $\mathbf{L_1}$ and $\mathbf{L_2}$ in showing the zinc recognition in live cells has also been demonstrated using HeLa cells as monitored by fluorescence imaging. The zinc complexes of $\mathbf{L_1}$ and $\mathbf{L_2}$ were isolated, and the structure of [$Zn\mathbf{L_1}$] has been established by single-crystal XRD and that of [$Zn\mathbf{L_2}$] by DFT calculations. TDDFT calculations were performed in order to demonstrate the electronic properties of receptors and their zinc complexes. The isolated zinc complexes, viz. [$Zn\mathbf{L_1}$] and [$Zn\mathbf{L_2}$], have been used as molecular tools for the recognition of anions on the basis of their binding affinities toward Zn^{2+}. [$Zn\mathbf{L_2}$] was found to be sensitive and selective toward phosphate-bearing ions and molecules and in particular to pyrophosphate (PPi) and ATP among the other 18 anions studied; however, [$Zn\mathbf{L_1}$] was not sensitive toward any of the anions studied. The selectivity has been shown on the basis of the changes observed in the emission and absorption spectral studies through the removal of Zn^{2+} from [$Zn\mathbf{L_2}$] by PPi. Thus, [$Zn\mathbf{L_2}$] has been shown to detect PPi up to 278 ± 10 ppb at pH 7.4 in aqueous methanolic (1/2 v/v) HEPES buffer.

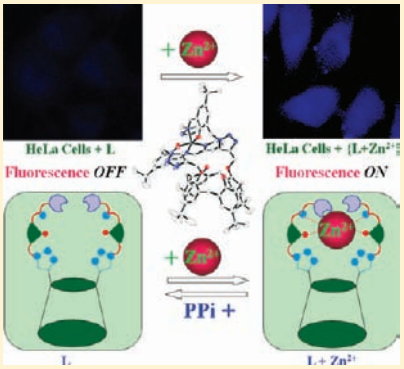

INTRODUCTION

Zn^{2+} is one of the most abundant transition-metal ions present in living cells, owing to its rich coordination chemistry.[1] Pools of labile Zn^{2+} are found in the cells of mammalian organs, including brain,[2] pancreas, and prostate.[3] Metabolic disorders of Zn^{2+} are responsible for various infections and diseases.[2,4,5] Zn^{2+} is also associated with various anions, especially with phosphates, by showing strong affinity.[6] Phosphate-based inorganic as well as organic molecules play fundamental roles in a wide range of chemical and biological processes of human life.[6] Among the phosphates, adenosine triphosphate (ATP) and inorganic pyrophosphate (PPi) have been of particular interest because of their role in certain chemical and biological processes such as energy storage, signal transduction, and DNA sequencing. In the DNA polymerase chain reaction, PPi is released; its detection is done as a real-time DNA sequencing method.[7] Biological fluids such as blood serum contain ~0.80–1.45 mM phosphates, and the higher phosphate levels are responsible for cardiovascular disease and acute renal failure.[8] Recently, metal ion complexes have been used as receptors for phosphates, and this emerged as one of the most successful strategies, since it provides specific metal ion–anion interactions.[9] Among the metal complex based receptors, the ones that exhibit fluorescence enhancement in the presence of Zn^{2+} have attracted considerable attention because of the strong affinity of Zn^{2+} toward phosphates.[10] Macrocyclic systems such as calix[4]arene have emerged as molecular scaffolds for building appropriate binding cores suitable for ion and molecular recognition owing to their wide topological features.[10−13] Our research group has been involved in the synthesis of various amide- and imine-based calix[4]arene conjugates for the selective recognition of ions and molecules.[14] We recently reported the selective detection of amino acids and anions using calix[4]arene conjugates bearing transition-metal ions.[14] Therefore, it is of prime interest to develop calix[4]-arene-based molecular systems to provide better sensitivity and selectivity toward ions and molecules. Thus, in the present paper, the synthesis and characterization of imino–phenolic–pyridyl conjugates of calix[4]arene, $\mathbf{L_1}$ and $\mathbf{L_2}$, and their selective recognition behavior toward Zn^{2+} have been reported. These conjugates were also demonstrated as potential live-cell fluorescence imaging agents upon treatment with Zn^{2+}. The differential recognition properties of the zinc complexes of these receptors, viz., [$Zn\mathbf{L_1}$] and [$Zn\mathbf{L_2}$], have been explored extensively using experimental and computational methods, particularly to sense PPi and ATP selectively among common biological phosphates.

Received: November 11, 2011
Published: April 20, 2012

   dx.doi.org/10.1021/ic202426v | *Inorg. Chem.* 2012, 51, 4994–5005

EXPERIMENTAL SECTION

General Information and Materials. ^{1}H and ^{13}C NMR spectra were measured on a Varian Mercury NMR spectrometer working at 400 MHz. The mass spectra were recorded on a Q-TOF Micromass instrument (YA-105) using electrospray ionization methods. Steady-state fluorescence spectra were measured on a Perkin-Elmer LS55 instrument. The absorption spectra were measured on a Varian Cary 100 Bio instrument. The diffraction data were collected on an Oxford Diffraction XCALIBUR-S diffractometer. All the perchlorate salts, viz., $NaClO_4·H_2O$, $KClO_4$, $Ca(ClO_4)_2·4H_2O$, $Mg(ClO_4)_2·6H_2O$, $Mn(ClO_4)_2·6H_2O$, $Fe(ClO_4)_2·xH_2O$, $Co(ClO_4)_2·6H_2O$, $Ni(ClO_4)_2·6H_2O$, $Cu(ClO_4)_2·H_2O$, $Zn(ClO_4)_2·6H_2O$, $Cd(ClO_4)_2·H_2O$, $Hg(ClO_4)_2·xH_2O$, and $Zn(OAc)_2·2H_2O$, were procured from Sigma Aldrich Chemical Co. (USA). Salts of different anions, viz., Bu_4NF, Bu_4NCl, Bu_4NBr, Bu_4NI, Bu_4NClO_4, $Bu_4NH_2PO_4$, Bu_4NHSO_4, $Na_4P_2O_7$, NaSCN, Na_2SO_4, Na_2CO_3, $NaNO_3$, $NaNO_2$, NaN_3, AMP, ADP, and ATP, were purchased from Sisco Research Laboratories Pvt Ltd. (India).

Bulk solutions of $\mathbf{L_1}$ and $\mathbf{L_2}$ and the metal salts were made up in MeOH, at 6×10^{-4} M concentration. The fluorescence studies performed in aqueous methanolic (1/2 v/v) HEPES buffer, pH 7.4 solution, always used a 50 μL amount of the bulk solution of $\mathbf{L_1}$ or $\mathbf{L_2}$ prepared at 6×10^{-4} M concentration in methanol. A 50 mM HEPES buffer stock solution was prepared with deionized water, and 1000 μL of this bulk solution was used for each titration of 3 mL of solution. During the metal ion titrations, the concentrations of metal perchlorates were varied accordingly to result in requisite mole ratios of metal ion to receptors, and the total volume of the solution was maintained at 3 mL in each case by the addition of CH_3OH and HEPES buffer. For anion titrations, the $[Zn\mathbf{L_1}]$ and $[Zn\mathbf{L_2}]$ were initially dissolved in the minimum amount of $CHCl_3$ (100 μL in 2 mL of bulk) and the final volumes were made up to 2 mL by adding methanol in order to get a final concentration of 6×10^{-4} M. Stock solutions of AMP, ADP, ATP, and PPi at 6×10^{-4} M concentration were made up in the HEPES buffer medium. During the anion titrations, the concentrations of anions were varied accordingly to result in requisite mole ratios of anions to zinc complexes, and the total volume of the solution was maintained at 3 mL in each case by the addition of appropriate volumes of CH_3OH and HEPES buffer solution. For absorption studies, the final concentrations of $\mathbf{L_1}$ and $\mathbf{L_2}$ were kept constant at 20 μM, and the procedure used for the titrations was the same as that used for fluorescence titrations. All the solvents used were procured from local sources and were dried and distilled by the usual procedures immediately before use. Distilled and deionized water was used for the studies. Quantum yields for the calix[4]arene conjugates, viz., $\mathbf{L_1}$ and $\mathbf{L_2}$, were measured in the absence and in the presence of Zn^{2+} using quinine sulfate as standard. Fluorescence and absorption titrations have also been carried out between these calix[4]arene conjugates, viz., $\mathbf{L_1}$ and $\mathbf{L_2}$ and zinc acetate (Supporting Information, Figures S1 and S2).

Computational Methodology. In the DFT calculations,[15] the initial model for $\mathbf{L_2}$ was prepared from the crystal structure of the complex $[Zn\mathbf{L_1}]$ upon using the following modifications: (a) removal of Zn^{2+}, (b) protonation of the salicyl OH moieties, and (c) introduction of one more $-CH_2$ group to the pyridyl moiety in each of the arms. This has been optimized by going through a cascade process starting from PM3 → HF/STO-3G → HF/3-21G → HF/6-31G → B3LYP/3-21G → B3LYP/6-31G. The output obtained at every stage has been given as the input for the next higher level of calculations. In order to create the neutral complex with Zn^{2+}, the salicyl OH groups were deprotonated and the resulting $\mathbf{L_2}^{2-}$ was used for further studies. The complex of $\mathbf{L_2}^{2-}$ with Zn^{2+} was made by simply placing the Zn^{2+} far away from the binding arms of the DFT optimized $\mathbf{L_2}^{2-}$ in such a way that the salicyl O and imine N atoms are pointed toward Zn^{2+}. To understand the electronic properties of $\mathbf{L_1}$, $\mathbf{L_2}$, and their Zn^{2+} complexes, TDDFT studies were carried out.[16] Single-point energies of the complexes formed were calculated using the formula $\Delta E_s = E_{[Zn^{2+}(L)]} - (E_L + E_{Zn^{2+}})$. In addition, the complex of PPi with Zn^{2+} was optimized with the B3LYP/6-31G(d,p) level and used for the single-point energy calculations (Supporting Information, Figure S3).

Cellular Imaging Methodology. Human cervical carcinoma (HeLa) cells were cultured in Eagle's Minimal Essential Medium (MEM) supplemented with 10% fetal bovine serum, 2.2 g/L sodium bicarbonate, and 1% antibiotic-antimycotic solution containing streptomycin, amphotericin B, and penicillin. Cells were maintained under a humidified atmosphere of 5% CO_2 and 95% air in a 37 °C incubator. Stock solutions (10 mM) of the conjugates of calix[4]arene were prepared in DMSO. HeLa cells were seeded at a density of 5×10^4 cells/mL in polylysine-coated glass-bottom cell culture dishes. After 24 h of seeding, MEM media was removed and the dishes were washed twice carefully with PBS. Cells were incubated in the presence of 10 μM (diluted in PBS) $\mathbf{L_1}$ and $\mathbf{L_2}$ separately for 20 min. Then, the PBS containing some traces of ligand was removed and the dishes were washed three times with PBS. At this stage, cells were imaged for the intrinsic fluorescence of the conjugates using an Eclipse TE 2000 U microscope (Nikon, Tokyo, Japan) at 40× magnification. Further, the cells were incubated with 10 μM $ZnSO_4$/pyrithione diluted in PBS buffer for 20 min. After this incubation, the PBS containing Zn^{2+} was removed and the cells were washed three times with PBS. Subsequently, different dishes were further incubated with 10 μM (diluted in PBS) of $\mathbf{L_1}$ and $\mathbf{L_2}$ separately for 20 min. After the incubation, the dishes were washed three times with PBS and the cells were imaged using an Eclipse TE 2000U microscope at 40× magnification. The exposure time was kept the same for all the cases. The images were processed using Image-Pro Plus software (Media Cybernetics, Silver Spring, MD).

Synthesis and Characterization of 1−3. Detailed information about the synthesis and characterization of compounds **1**−**3** is given in Supporting Information.

Synthesis and Characterization of 4.[14e] A mixture of potassium carbonate (5.10 g, 36.72 mmol) and *p-tert*-butylcalix[4]arene (10.0 g, 15.43 mmol) in dry acetone (200 mL) was stirred at room temperature for 1 h. A solution of propargyl bromide (6.49 g, 30.80 mmol) in dry acetone (50 mL) was added dropwise into this stirred mixture over a period of 30 min. The reaction mixture was refluxed for 24 h and was then cooled to room temperature. The reaction mixture was filtered over Celite to remove insoluble particles, and the filtrate was concentrated by a rotary evaporator. A 100 mL portion of 2 M HCl was added to the concentrated reaction mixture, and the product was extracted with dichloromethane (3 × 100 mL). The combined organic extracts were successively washed with water and brine (100 mL), dried over anhydrous Na_2SO_4, filtered, and evaporated to dryness in vacuo. The crude product was recrystallized from CH_2Cl_2/CH_3OH to afford **4** as a white solid (9.10 g, 82% yield). ^{1}H NMR (400 MHz, $CDCl_3$): δ (ppm) 7.07 (s, 4H, Ar-H), 6.73 (s, 4H, Ar-H), 6.50 (s, 2H, OH), 4.74 (d, J = 2.4 Hz, 4H, OCH_2), 4.37 (d, J = 13.4 Hz, 4H, $ArCH_2Ar$), 3.33 (d, J = 13.4 Hz, 4H, $ArCH_2Ar$), 2.54 (t, J = 2.4 Hz, 2H, C≡CH), 1.30 (s, 18H, $(CH_3)_3$), 0.90 (s, 18H, $(CH_3)_3$). ^{13}C NMR ($CDCl_3$, 100 MHz): δ (ppm) 150.51, 149.62, 147.40, 141.77, 132.74, 128.16, 125.70, 125.19, 78.93, 63.45, 34.05, 34.02, 32.19, 31.88, 31.11. HRMS: m/z calcd for $C_{50}H_{60}O_4$ (M + H) 725.4570, found 725.4576.

Synthesis and Characterization of 5. Compound **4** (4.0 g, 5.52 mmol) was added to a solution of **3** (2.83 g, 12.70 mmol) in 50 mL of a dichloromethane and water (50/50) mixture. To this solution were added $CuSO_4·5H_2O$ (165.38 g, 0.662 mmol) and sodium ascorbate (437.4 mg, 22.08 mmol). The resulting solution was stirred for 12 h at room temperature. Upon completion of the reaction, as checked on the basis of TLC, the organic layer was separated and the aqueous layer was extracted with dichloromethane (2 × 50 mL). The combined organic layer was washed with water and then with brine (2 × 50 mL) and dried over anhydrous Na_2SO_4, and the solvent was removed in vacuo. The crude product was purified by triturating with hexane followed by filtering the precipitate. Yield: 81%. ^{1}H NMR ($CDCl_3$, 400 MHz): δ (ppm) 11.30 (s, 2H, Sal-OH), 9.83 (s, 2H, sal-CHO), 8.08 (s, 2H, triazole-H), 7.62 (s, 2H, Sal-H) 7.49 (d, 2H, Sal-H), 7.15 (s, 2H, Ar-OH), 6.98 (s, 4H, Ar-H), 6.77 (s, 4H, Ar-H), 5.56 (s, 4H, Sal-CH2), 5.18 (s, 4H, Ar-O-CH_2), 4.14 (d, J = 13.0 Hz, 4H, $ArCH_2Ar$), 3.17 (d, J = 13.0 Hz, 4H, $ArCH_2Ar$), 1.27 (s, 18H, Ar-$(CH_3)_3$), 1.26 (s,

dx.doi.org/10.1021/ic202426v | Inorg. Chem. 2012, 51, 4994−5005

Scheme 1. Synthesis of the Precursors and the Final Receptor Molecules, L_1 and L_2[a]

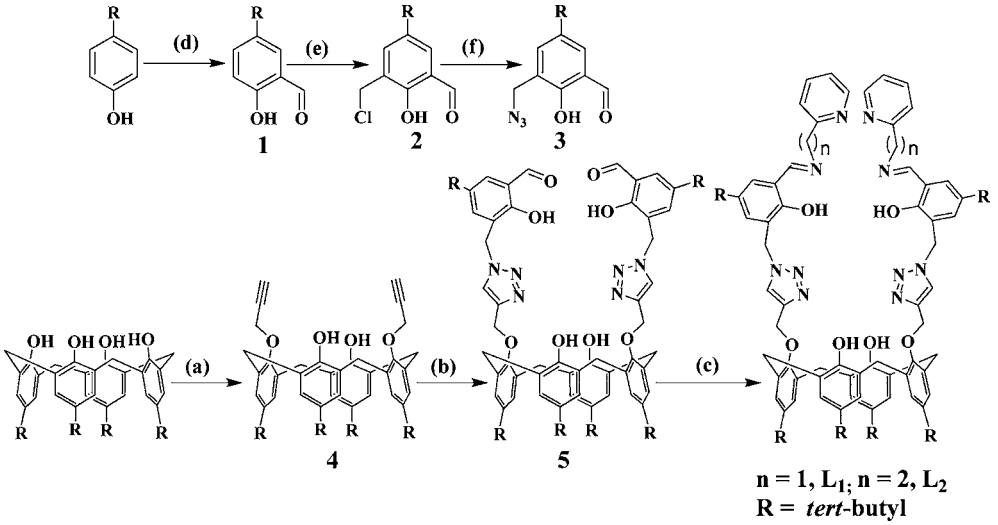

[a]Synthesis of L_1 and L_2: (a) propargyl bromide, K_2CO_3, acetone, reflux, 24 h; (b) 5-*tert*-butyl-3-(azidomethyl)-2-hydroxybenzaldehyde (**3**), $CuSO_4 \cdot 5H_2O$, and sodium ascorbate in dichloromethane/water (1/1), room temperature, 12 h; (c) pyridin-2-ylmethanamine or 2-(pyridin-2-yl)ethanamine, methanol, room temperature, 8 h; (d) $SnCl_4$, Bu_3N, $OH(CH_2O)_nH$, dry toluene, reflux; (e) 37% formaldehyde, concentrated HCl, room temperature, 48 h; (f) NaN_3, DMF, room temperature, 12 h.

18H, Ar-$(CH_3)_3$), 0.96 (s, 18H, Sal-$(CH_3)_3$). ^{13}C NMR ($CDCl_3$, 100 MHz): δ (ppm) 196.6, 157.1, 150.4, 149.6, 147.2, 144.2, 143.2, 141.5, 135.3, 132.6, 130.7, 127.8, 125.6, 125.0, 124.2, 123.1, 120.2, 69.8, 48.2, 34.2, 33.9, 33.8, 31.7, 31.2, 31.1, 31.02. IR: ν 3463, 2959, 1656, 1483 cm^{-1}. HRMS (ESI): m/z calcd for $C_{74}H_{90}N_6O_8$ $[M + H]^+$ 1191.6898, found 1191.6898.

Synthesis and Characterization of L_1. A mixture of **5** (1.0 g, 0.839 mmol) and pyridin-2-ylmethanamine (0.182 g, 1.68 mmol) in methanol was stirred for 8 h, which gives rise to a yellow precipitate. The precipitate was filtered under vacuum to get a yellow solid, which was further recrystallized using methanol to get pure solid product L_1. Yield: 83%, ^{1}H NMR ($CDCl_3$, 400 MHz): δ (ppm) 13.6 (broad s, 2H, Sal-OH), 8.54 (m, 2H, Py-H, J = 4.88 Hz), 8.5 (s, 2H, imine-H), 8.0 (s, 2H, triazole-H), 7.60 (t, 2H, Py-H, J = 7.9 Hz), 7.42 (t, 2H, Py-H), 7.25−7.27 (m, 4H, Sal-H), 7.16 (t, 2H, Py-H), 7.16 (s, 2H, Ar-OH), 6.95 (s, 4H, Ar-H), 6.7 (s, 4H, Ar-H), 5.6 (s, 4H, Ar-OCH_2), 5.1 (s, 4H, Sal-CH_2), 4.85(s, 4H, Py-CH_2), 4.12 (d, 4H, Ar-CH_2-Ar, J = 13.1 Hz), 3.12 (d, 4H, Ar-CH_2-Ar, J = 13.1 Hz), 1.26 (s, 18H, Ar-$C(CH_3)_3$), 1.24 (s, 18H, Sal-$(CH_3)_3$), 0.92 (s, 18H, Ar-$C(CH_3)_3$). ^{13}C NMR ($CDCl_3$, 100 MHz): δ (ppm) 166.93, 157.75, 157.13, 150.5, 149.6, 149.4, 147.0, 144.0, 141.62, 141.44, 137.0, 132.60, 130.82, 128.98, 127.83, 125.60, 125.0, 124.23, 122.44, 122.26, 122.0, 118.23, 69.73, 64.80, 48.90, 34.04, 33.91, 33.83, 31.73, 31.38, 31.00. ES/MS: m/z 1371.5 ($[M]^+$, 100%). HRMS: m/z calcd for $C_{86}H_{102}N_{10}O_6$ 1371.8062, found 1371.8115.

Synthesis and Characterization of L_2. L_2 was prepared by using the procedure given for L_1, but with 2-(pyridin-2-yl)ethanamine. Yield: 89%. ^{1}H NMR (DMSO-d_6, 400 MHz): δ (ppm) 13.9 (broad s, 2H, Sal-OH), 8.53 (s, 2H, imine-H), 8.48 (d, 2H, Py-H, J = 4.8 Hz), 8.0 (s, 2H, triazole-H), 7.9 (s, 2H, Ar-OH), 7.7 (t, 2H, Py-H), 7.42 (d, 2H, Sal-H), 7.37 (d, 2H, Sal-H), 7.23−7.17 (m, 4H, Py-H), 7.0 (s, 4H, Ar-H), 6.9 (s, 4H, Ar-H), 5.60 (s, 4H, Ar-OCH_2), 5.0 (s, 4H, Sal-CH_2), 3.98 (d, 4H, Ar-CH_2-Ar, J = 12.8 Hz), 3.90 (t, 4H, N-CH_2-Py), 3.17 (d, 4H, Ar-CH_2-Ar, J = 12.8 Hz), 3.04 (t, 4H, N-CH_2-Py), 1.18 (s, 18 H, Ar-$C(CH_3)_3$), 1.14 (s, 18 H, Sal-$(CH_3)_3$), 1.05 (s, 18H, Ar-$C(CH_3)_3$). ^{13}C NMR ($CDCl_3$, 100 MHz): δ (ppm) 165.40, 158.95, 157.47, 150.50, 149.63, 149.47, 147.00, 143.88, 141.43, 141.21, 136.49, 132.56, 130.51, 128.52, 127.84, 125.57, 125.00, 124.22, 123.78, 122.45, 121.56, 118.05, 69.77, 58.66, 48.92, 39.33, 33.99, 33.91, 33.81, 31.72, 31.37, 31.0. ES/MS: m/z 1400.13 ($[M + 1]^+$, 100%). HRMS: m/z calcd for $C_{88}H_{106}N_{10}O_6$ 1399.8381, found 1399.8375.

Synthesis and Characterization of [ZnL$_1$]. To a solution of L_1 (0.150 g, 0.109 mmol) in $CHCl_3$ (6 mL) was added a methanolic solution of $Zn(CH_3COO)_2 \cdot 2H_2O$ (0.026 g, 0.120 mmol, 5 mL), and the resulting reaction mixture was refluxed for 5 h. After the solution was concentrated, a light yellow precipitate started to form and the solid that formed was then filtered, washed with cold methanol, and dried in vacuo to give the desired product, [ZnL_1]. Yield: 92%, ^{1}H NMR ($CDCl_3$, 400 MHz): δ (ppm) 9.23 (s, 2H, imine-H), 8.04 (s, 2H, triazole-H), 7.9 (d, 2H, Py-H), 7.70 (s, 2H, Ar-OH), 7.61 (broad d, 2H, Sal-H), 7.36 (t, 2H, Py-H), 6.83−6.9 (m, 10H, Ar-H, Py-H), 6.60 (dd, 4H, Sal-H, Py-H), 5.6 (s, 4H, Ar-OCH_2), 5.12 (d, 2H, Sal-CH_2), 5.02 (d, 2H, Py-CH_2), 4.33 (d, 2H, Sal-CH_2), 4.15 (d, 2H, Py-CH_2), 3.55 (d, 2H, Ar-CH_2-Ar), 3.44 (d, 2H, Ar-CH_2-Ar), 2.78 (d, 2H, Ar-CH_2-Ar), 2.31(d, 2H, Ar-CH_2-Ar), 1.36 (s, 18H, Ar-$C(CH_3)_3$), 1.19 (S, 18H, Sal-$(CH_3)_3$), 1.02 (s, 18H, Ar-$C(CH_3)_3$). ^{13}C NMR ($CDCl_3$, 100 MHz): δ (ppm) 170.95, 167.84, 156.05, 150.45, 148.46, 148.40, 147.31, 143.08, 141.32, 137.42, 134.96, 133.72, 133.36, 133.23, 132.70, 127.92, 127.65, 127.47, 126.91, 126.19, 125.48, 125.07, 124.67, 122.73, 121.90, 117.51, 69.65, 61.76, 51.98, 34.10, 33.86, 33.81, 31.88, 31.71, 31.54, 31.17. HRMS: m/z calcd for $C_{86}H_{100}N_{10}O_6Zn$ 1433.7197, found 1433.7190. Crystal data for [ZnL_1]: empirical formula $C_{88}H_{96}N_{10}O_9Zn$; formula weight 1503.12; temperature 150(2) K; radiation Mo Kα; wavelength/Å 0.710 73; crystal system triclinic, $P\bar{1}$; unit cell dimensions a = 11.0065(3) Å, b = 16.4816(7) Å, and c = 24.5981(10) Å; α = 106.453(4)°, β = 90.525(3)°, γ = 93.464(3)°; V = 4270.1(3) Å^3; Z = 2; D_{calc}= 1.169 g/cm^3; μ = 0.348 mm^{-1}; $F(000)$ = 1592; θ = 3.33, 25.0°(min, max); no. of unique reflections 14 984; no. of parameters 991; R_{obs} = 0.0873, $wR2_{obs}$ = 0.2147; GOF = 1.005.

Synthesis and Characterization of [ZnL$_2$]. This complex has been synthesized by adapting the same procedure that was used for [ZnL_1] but using L_2 instead of L_1. Yield: 86%. ^{1}H NMR (DMSO-d_6, 400 MHz): δ (ppm) 8.7 (s, 2H, imine-H), 8.4 (d, 2H, Py-H, J = 4.8 Hz), 8.23 (s, 2H, Ar-OH), 8.13 (s, 2H, triazole-H), 7.7 (t, 2H, Py-H), 7.35 (d, 2H, Sal-H), 7.16 (t, 2H, Py-H), 6.9−7.0 (m, 12H, PyH, Sal-H, Ar-H), 5.66 (broad d, 4H, Ar-OCH_2), 4.95 (s, 4H, Sal-CH_2), 3.91 (broad d, 8H, Ar-CH_2-Ar, Py-NCH_2, J = 12.8 Hz), 3.67 (broad d, 8H, Ar-CH_2-Ar, Py-NCH_2, J = 12.8 Hz), 1.20 (s, 18 H, Ar-$C(CH_3)_3$), 1.16 (s, 18 H, Sal-$(CH_3)_3$), 1.09 (s, 18H, Ar-$C(CH_3)_3$). ^{13}C NMR ($CDCl_3$, 100 MHz): δ (ppm) 171.45, 166.20, 158.10, 150.35, 149.33, 149.08, 147.10, 143.98, 141.52, 137.01, 136.42, 132.99, 132.87, 132.45, 132.27, 127.99, 127.60, 127.47, 125.63, 125.14, 124.99, 123.67, 121.87, 117.55, 69.79, 59.57, 50.44, 38.27, 33.95, 33.82, 33.70, 31.74, 31.40, 31.01. HRMS: m/z calcd for $C_{88}H_{104}N_{10}O_6Zn$ 1461.7498, found 1461.7510.

dx.doi.org/10.1021/ic202426v | Inorg. Chem. 2012, 51, 4994−5005

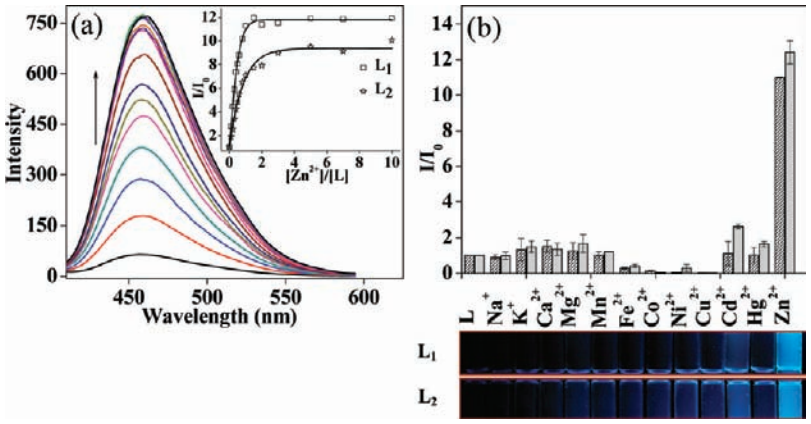

Figure 1. Fluorescence titration of L_1 and L_2 by metal ions. (a) Fluorescence spectra obtained during the titration of L_1 with Zn^{2+} in aqueous methanolic (1/2 v/v) HEPES buffer (pH 7.4), λ_{ex} 390 nm. The inset shows the relative fluorescence intensity (I/I_0) as a function of $[Zn^{2+}]/[L_1$ or $L_2]$ mole ratio. (b) Histogram showing the fluorescence response of various metal ions with L_1 (gray bars) and L_2 (bars with hash marks) and the vials exhibiting visual color changes of L_1 and L_2 in the presence of these ions under 365 nm incident light.

RESULTS AND DISCUSSION

Imino−phenolic−pyridyl conjugates of calix[4]arene, L_1 and L_2, were synthesized in three consecutive steps starting from *p-tert*-butylcalix[4]arene followed by the preparation of its dipropargyl ether and the triazole-linked conjugate, as shown in Scheme 1. The precursor azide derivative **3** has been synthesized in three steps[14i,17] (Supporting Information) starting from *p-tert*-butylphenol (Scheme 1). The receptor molecules L_1 and L_2 have been synthesized by the condensation of **5** with pyridin-2-ylmethanamine and 2-(pyridin-2-yl)ethanamine, respectively. The zinc complexes of these conjugates have been isolated in quantitative yield by reacting L_1 or L_2 with zinc acetate in methanol, as detailed in the Experimental Section. All the precursor and receptor molecules were characterized by various analytical and spectral techniques. The conjugates of calix[4]arene were found to be in a cone conformation on the basis of NMR studies (Experimental Section and Supporting Information, Figures S4−S9). The molecular structure of the zinc complex of receptor L_1 has been established on the basis of single-crystal XRD data, and the structure of $[ZnL_2]$ has been optimized using DFT calculations.

Zn^{2+} Recognition. The sensitivity of L_1 and L_2 toward different metal ions and their preferential selectivity toward Zn^{2+} over the other ions has been studied by fluorescence and absorption titrations.

Fluorescence Titrations of L_1 and L_2 by Metal Ions. The receptors L_1 and L_2 exhibit very weak emission at ∼455 nm when excited at 390 nm in 1/2 water/methanol mixture at pH 7.4 to have an effective HEPES buffer concentration of 10 mM. Titration of L_1 or L_2 with Zn^{2+} results in the enhancement of fluorescence intensity as a function of the added Zn^{2+} concentration (Figure 1a). A plot of fluorescence intensity as a function of added $[Zn^{2+}]/[L]$ mole ratio (Figure 1a, inset) shows a stoichiometry of 1/1 between the receptor and Zn^{2+} and the intensity saturates at ≥1 equiv. The observed fluorescence enhancement may be viewed as follows. The calix[4]arene conjugates, viz., L_1 and L_2, exhibit low fluorescence owing to the isomerization of the imine (C═N bond) as well as to the excited-state proton transfer (ESPT) from salicyl −OH to the imine nitrogen in the excited state, which has been well documented in the literature in the case of Schiff base molecular systems. When such Schiff base connected calix[4]arene conjugates bind to Zn^{2+}, these processes are inhibited to result in fluorescence enhancement.[18] The binding of Zn^{2+} to these conjugates has also been delineated from other spectral methods, as reported in this paper. Even the chelation by Zn^{2+} to the imine N, phenolic O, and pyridyl N brings rigidity to the conjugates and results in chelation-enhanced fluorescence (CHEF). During the chelation process, the phenolic −OH from the salicyaldimine moiety is deprotonated and forms a six-membered chelate ring. The binding affinities of Zn^{2+} toward L_1 and L_2 have been calculated from the Benesi−Hildebrand equation and found to have association constants of $[9.3(\pm0.11)] \times 10^4$ and $[7.2(\pm0.09)] \times 10^4$ M^{-1}, respectively. A 30% increase observed in the association constant in the case of L_1 as compared to L_2 speaks for the stronger binding of Zn^{2+} with L_1, as explained on the basis of the coordination cores later in this paper.

In order to check whether L_1 and L_2 are sensitive to only Zn^{2+} or even to the other ions, fluorescence titrations were carried out in the same medium with 12 different metal ions, viz. Na^+, K^+, Mg^{2+}, Ca^{2+}, Mn^{2+}, Fe^{2+}, Co^{2+}, Ni^{2+}, Cu^{2+}, Cd^{2+}, and Hg^{2+}, and no significant fluorescence enhancement was found in the presence of these ions (Figure 1b). Minimum detectable concentrations of ∼31 and ∼112 ppb of Zn^{2+} for L_1 and L_2, respectively, has been detected by the fluorescence titrations carried out by keeping the receptor to Zn^{2+} mole ratio as 1/1 (Supporting Information, Figure S10). Therefore, L_1 and L_2 can be used for the selective recognition of Zn^{2+} among the 12 different metal ions studied. The titrations carried out at different pHs of the medium exhibited no variation in the fluorescence intensity in the pH range 6−10. However, at highly acidic and basic pH, the fluorescence of these conjugates and their Zn^{2+} complexes shows a decreas,e indicating the instability of the complex under these conditions (Supporting Information, Figure S11). The quantum yields of L_1 and L_2 were found to be 0.024 and 0.020, respectively, and those of their Zn^{2+} complexes show higher ϕ values of 0.190 and 0.165, respectively. The observed 8-fold increase in the quantum yield of the Zn^{2+}-bound species, the presence of water and buffer in the medium of measurements, and the observed low detection limits seem to qualify L_1 and L_2 for sensing as well as quantifying Zn^{2+} by switch-on fluorescence at physiological pH. Under UV light, the solutions of L_1 and L_2 are nonfluorescent, whereas in the presence of Zn^{2+} an intense blue fluorescent

dx.doi.org/10.1021/ic202426v | *Inorg. Chem.* 2012, 51, 4994−5005

color was observed (Figure 1b, bottom) and no such fluorescent color was observed in case of the other metal ions. Thus, Zn^{2+} can easily be differentiated by its fluorescent color change from the other metal ions.

The selectivity of Zn^{2+} has been studied by carrying out appropriate competitive metal ion titrations in the presence of alkali and alkaline-earth ions (being major components of biological fluids) and also Cd^{2+} and Hg^{2+} (being environmentally toxic), and no significant change was found in the fluorescence enhancement when Zn^{2+} interacted with $\mathbf{L_1}$ and $\mathbf{L_2}$ in the presence of different ions. The marginal fluorescence quenching observed in the presence of Cd^{2+} and Hg^{2+} may be considered as a heavy atom effect upon interaction with the excited species. However, the fluorescence of these is completely quenched in the presence of Cu^{2+}. Thus, $\mathbf{L}$ can be used for the selective recognition of Zn^{2+} in the presence of most of the metal ions except Cu^{2+} (Supporting Information, Figure S12).

Absorption Titration of L_1 and L_2 by Zn^{2+}. The absorption spectra of free $\mathbf{L_1}$ and $\mathbf{L_2}$ in aqueous methanolic (1/2 v/v) HEPES buffer (pH 7.4) exhibited different bands from 200 to 450 nm. Upon the addition of Zn^{2+}, a new band was observed at ~385 nm in case of $\mathbf{L_1}$ and at 375 nm in case of $\mathbf{L_2}$, and their absorbance increases. The absorbance of the other two bands in the case of $\mathbf{L_1}$ (~330 and ~440 nm) and $\mathbf{L_2}$ (325 and 425 nm) decreases. The isosbestic points observed in the cases of $\mathbf{L_1}$ (345 and 425 nm) and $\mathbf{L_2}$ (340 and 415 nm) were indicative of the transition between the free and the complexed species (Figure 2). The stoichiometry of the complex formed

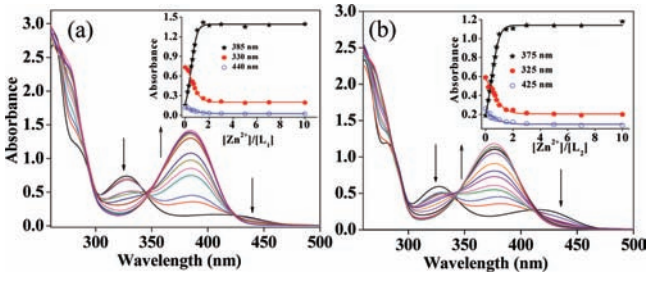

Figure 2. Absorption titration of receptors by Zn^{2+} in aqueous methanol (1/2 v/v) HEPES buffer (pH 7.4): (a) spectra obtained for $\mathbf{L_1}$; (b) spectra obtained for $\mathbf{L_2}$. The insets show the plot of absorbance vs $[Zn^{2+}]/[\mathbf{L}]$ for different absorption bands for both (a) $\mathbf{L_1}$ and (b) $\mathbf{L_2}$.

between the receptors and Zn^{2+} has been derived to be 1/1 on the basis of a Jobs plot (Supporting Information, Figure S13). The binding affinities of Zn^{2+} toward $\mathbf{L_1}$ and $\mathbf{L_2}$ have also been calculated from the Benesi–Hildebrand equation using absorption data and found to have the association constants of $[6.8(\pm0.5)] \times 10^4$ and $[3.7(\pm0.17)] \times 10^4$ M^{-1}, respectively.

Electrospray Mass Spectrometry. ESI mass spectra obtained for the isolated complexes of $\mathbf{L_1}$ and $\mathbf{L_2}$ with Zn^{2+} resulted in molecular ion peaks at m/z 1433.72 and 1461.75, respectively (Supporting Information, Figures S8 and S9). The isotopic peak patterns observed for these peaks are characteristic of the presence of zinc, thus supporting the complex formation of Zn^{2+} with $\mathbf{L_1}$ and $\mathbf{L_2}$ (Figure 3).

^{1}H NMR Studies. ^{1}H NMR spectral measurements of $\mathbf{L_1}$ and $\mathbf{L_2}$ and their Zn^{2+} complexes were carried out (Figure 4 and Supporting Information, Figures S6–S9). Upon the interaction of $\mathbf{L_1}$ or $\mathbf{L_2}$ with Zn^{2+}, the imine H, phenolic OH, Py H, and

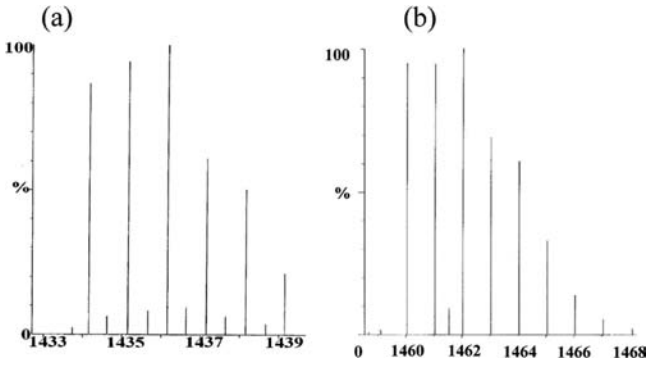

Figure 3. Molecular ion peak observed in ESI MS with its isotopic peak pattern: (a) $[Zn\mathbf{L_1}]$; (b) $[Zn\mathbf{L_2}]$.

bridging and arm CH_2 protons showed minimal to marginal changes in their δ values. The absence of any changes observed in the chemical shift of the triazole proton rules out interactions between it and Zn^{2+}. Considerable shifts observed in the Py CH_2 and Py H protons supports the binding of the pyridyl moiety. All these changes are suggestive of the complex formation of $\mathbf{L_1}$ and $\mathbf{L_2}$ with Zn^{2+} by utilizing both of its chelating arms.

Structures of the Zinc Complexes. While the structure of $[Zn\mathbf{L_1}]$ could be established crystallographically owing to the availability of nicely diffracting single crystals, the same had to be established by DFT computational methods in the case of $[Zn\mathbf{L_2}]$, as no single crystals could be obtained.

Single-Crystal XRD Structure of $[ZnL_1]$. Single crystals of $[Zn\mathbf{L_1}]$ suitable for X-ray diffraction were obtained by slow diffusion of methanol into a solution of $[Zn\mathbf{L_1}]$ in chloroform. It crystallizes in the triclinic system with space group $P\bar{1}$. The details of the data collection and the structure refinement are given in the Experimental Section. The calix[4]arene unit adopts a cone conformation by forming intramolecular O–H···O hydrogen bonds at the lower rim. In the crystal structure of $[Zn\mathbf{L_1}]$, it is observed that one of the coordinating arms is bent toward the calix[4]arene cavity and the other arm projects from the top by forming an N_3O_2 core to coordinate Zn^{2+} (Figure 5). The structure shows that Zn^{2+} has a square-pyramidal geometry formed by using two phenolic oxygens, two imine nitrogens of both the arms, and one pyridyl nitrogen from one of the arms. In the lattice of $[Zn\mathbf{L_1}]$, the two calix[4]arene units form a dimerlike structure at the lower rim through weak hydrogen bonding of the types O–H···N and O–H···O, mediated via two water molecules (Figure 6), wherein the two Zn^{2+} centers are separated by 7.55 Å. Further, these dimers were again stacked in its lattice and exhibit both hydrophobic and hydrophilic columnar stacked patterns formed by the *tert*-butyl part of the calix[4]arene and the lower rim of the zinc binding portion, respectively (Supporting Information, Figures S14 and S15, Tables S1 and S2).

Structure of $[ZnL_2]$ by Computational Modeling. Computational calculations were carried out using the Gaussian 03 package[15] in order to establish the complexation features of $\mathbf{L_2}$ by Zn^{2+}. In the optimized structure of $[Zn\mathbf{L_2}]$ (Figure 7 and Supporting Information, Tables S3 and S4), the Zn^{2+} was found in an N_3O_2 core as was observed in the case of $[Zn\mathbf{L_1}]$, where the second pyridyl nitrogen group is disposed at a distance of 5.65 Å, but with a greater distortion in the geometry. The comparison of the metric data of the coordination spheres of both complexes clearly supports this through an elongated

dx.doi.org/10.1021/ic202426v | *Inorg. Chem.* 2012, 51, 4994–5005

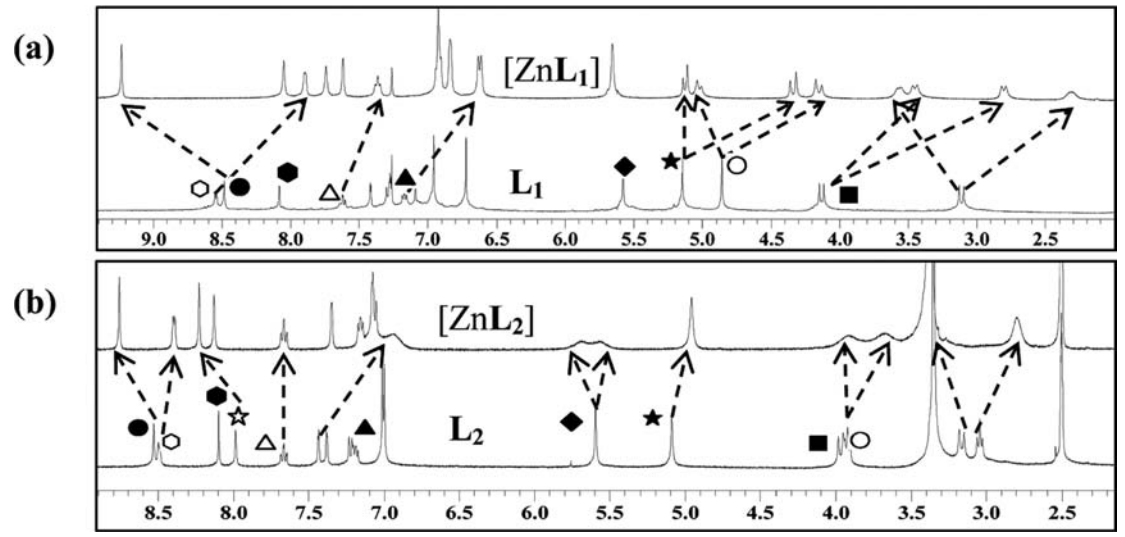

Figure 4. (a) ^{1}H NMR spectra of $\mathbf{L_1}$ and [Zn$\mathbf{L_1}$]. (b) ^{1}H NMR spectra of $\mathbf{L_2}$ and [Zn$\mathbf{L_2}$]. Legend: (●) imine-H; (⬡, ▲, △) Py H; (★) CH_2 connecting to triazole with aldimine; (♦) CH_2 connecting to calix[4]arene with triazole; (○) Py CH_2; (■) calix[4]arene bridging CH_2; (☆) Calix OH; (⬢) triazole H.

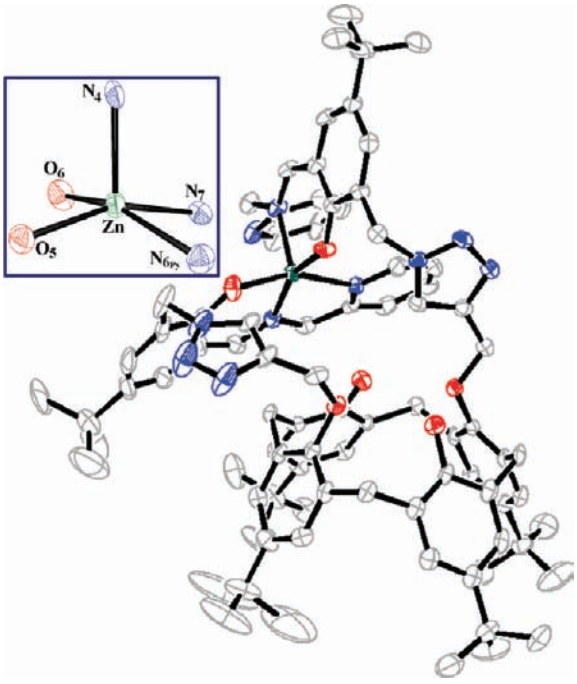

Figure 5. ORTEP diagram of [Zn$\mathbf{L_1}$] drawn with 50% probability ellipsoids. The inset shows the coordination sphere around the zinc ion. Hydrogen atoms are omitted for clarity. Bond lengths (Å) and bond angles (deg) in the coordination sphere: Zn−N_6 = 2.130(5), Zn−N_7 = 2.071(5), Zn−N_4 = 2.049(4), Zn−O_5 = 1.989(3), Zn−O_6 = 1.985(5); O_5−Zn−O_6 = 92.24(17), O_5−Zn−N_6 = 93.37(17), O_5−Zn−N_7 = 158.50(16), O_5−Zn−N_4 = 94.06(16), O_6−Zn−N_6 = 157.52(17), O_6−Zn−N_7 = 89.44(19), O_6−Zn−N_4 = 101.44(19), N_6−Zn−N_7 = 77.60(19), N_6−Zn−N_4 = 99.86(18), N_7−Zn−N_4 = 106.62(18).

PyN−Zn bond observed in the case of [Zn$\mathbf{L_2}$] as compared to that in [Zn$\mathbf{L_1}$].

Binding Core Comparison and Conformational Changes Observed in the Arms. A careful examination of the binding cores of both the structures reveals that the Zn^{2+} center is more distorted in the case of [Zn$\mathbf{L_2}$] as compared to its homologue [Zn$\mathbf{L_1}$], with a major change being reflected in lengthening the PyN−Zn bond in the case of the former (Figure 8 and Supporting Information, Tables S3−S7). This has further resulted in the lowering of crowding by the pyridyl moiety at the Zn^{2+} center in [Zn$\mathbf{L_2}$]. Only marginal differences are observed in the dihedral angles (Supporting Information, Figure S16 and Table S8) of the arms on going from [Zn$\mathbf{L_1}$] to [Zn$\mathbf{L_2}$], while the arms move farther apart in comparison to their free ligands in order to accommodate the Zn^{2+} in the binding core formed by the two salicylimine, two phenolic, and one pyridyl moiety, as was also observed in the crystal structure of [Zn$\mathbf{L_1}$]. All of this can be reconciled by the higher K_{assoc} value observed with [Zn$\mathbf{L_1}$] as compared to that of [Zn$\mathbf{L_2}$].

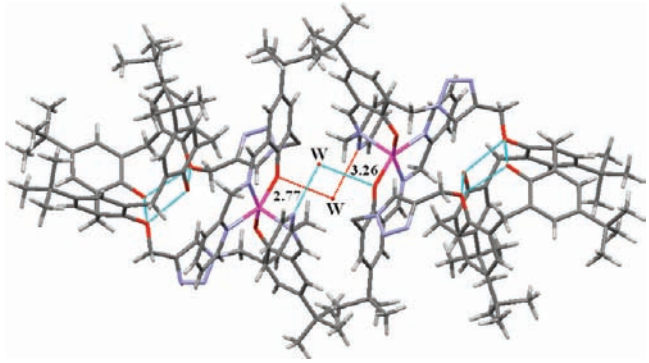

Figure 6. Dimer of [Zn$\mathbf{L_1}$] formed in the lattice via intermolecular hydrogen bonding mediated through water molecules. W = water oxygen.

Computational Studies of [Zn$\mathbf{L_1}$] and [Zn$\mathbf{L_2}$] by Time-Dependent Density Functional Theory. TDDFT calculations were performed to explain the electronic properties of these complexes in their ground and excited states. The vertical transitions calculated by TDDFT (Supporting Information, Tables S9 and S10) were compared with the solid-state UV−vis diffuse reflectance spectra of [Zn$\mathbf{L_1}$] and [Zn$\mathbf{L_2}$] and were found to have good agreement with the experimental data.[16] The TDDFT calculations performed at the B3LYP/6-31G(d,p) level of theory revealed the absorption bands in the region of

dx.doi.org/10.1021/ic202426v | Inorg. Chem. 2012, 51, 4994−5005

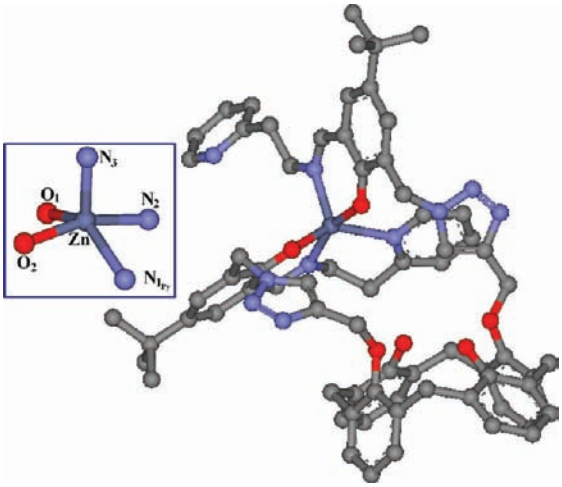

Figure 7. B3LYP/6-31G(d,p) optimized structure of [Zn$\mathbf{L}_2$]. The inset shows the coordination sphere around the zinc ion. Bond lengths (Å) and bond angles (deg) in the coordination sphere: Zn−N_1 = 2.35, Zn−N_2 = 2.07, Zn−N_3 = 2.05, Zn−O_1 = 2.00, Zn−O_2 = 1.98; O_1−Zn−O_2 = 87.21, O_1−Zn−N_1 = 141.60, O_1−Zn−N_2 = 88.29, O_1−Zn−N_3 = 112.42, O_2−Zn−N_1 = 86.00, O_2−Zn−N_2 = 161.00, O_2−Zn−N_3 = 93.42, N_1−Zn−N_2 = 86.09, N_1−Zn−N_3 = 105.68, N_2−Zn−N_3 = 105.34.

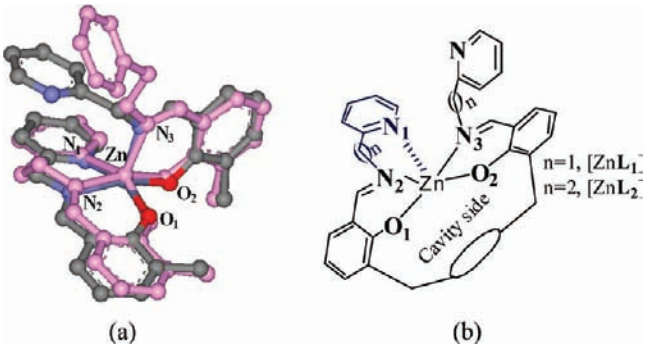

Figure 8. Comparison of the binding cores around zinc in [Zn$\mathbf{L}_1$] and [Zn$\mathbf{L}_2$]: (a) overlap of the binding core of the structures of [Zn$\mathbf{L}_1$] (gray) and [Zn$\mathbf{L}_2$] (pink); (b) schematic diagram of the binding core.

λ_{max} 270−400 nm (Figure 9). The studies suggest that the vertical transitions observed at ∼369 and ∼354 nm are comparable with those from experimental data for [Zn$\mathbf{L}_1$] and [Zn$\mathbf{L}_2$], respectively. In both cases, the highest observed oscillator strengths (F) correspond to the experimental λ_{max} (at ∼369 and ∼354 nm), which is assigned to the transition A that results from $\pi \rightarrow \pi^*$ of the salicylimine and pyridyl fragments of the arms (Figure 9, Supporting Information, Table S9 and S10). Corresponding molecular orbitals (MOs) of the two one-electron excitations are shown in Figure 10 and the Supporting Information (Figure S17). These MOs are mostly localized on the salicylimine and pyridyl parts of [Zn$\mathbf{L}_1$] and [Zn$\mathbf{L}_2$], and the percentages of localization are given in the Supporting Information (Table S9 and S10). Similar studies have also been carried out for $\mathbf{L}_1$ and $\mathbf{L}_2$, and the corresponding electronic transition data have been given in the Supporting Information (Figures S18 and S19 and Tables S11 and S12).

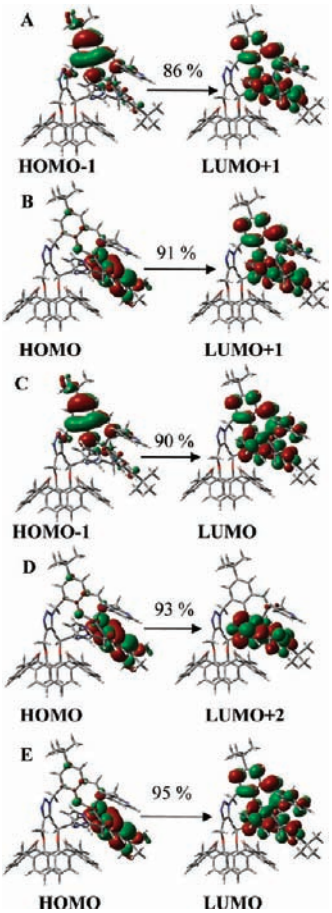

Figure 10. Pictorial representation of the molecular orbitals (MOs) calculated for the singlet vertical electronic transitions A−E (given in the Supporting Information, Table S9) using TDDFT for [Zn$\mathbf{L}_1$]. Contributions of key transition MOs are given above the arrows as percentages.

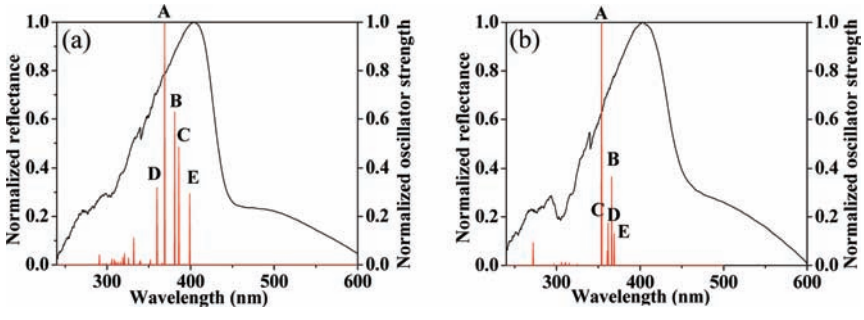

Figure 9. Normalized TDDFT singlet monoelectronic vertical transitions and normalized diffuse reflectance spectra: (a) [Zn$\mathbf{L}_1$]; (b) [Zn$\mathbf{L}_2$].

dx.doi.org/10.1021/ic202426v | *Inorg. Chem.* 2012, 51, 4994−5005

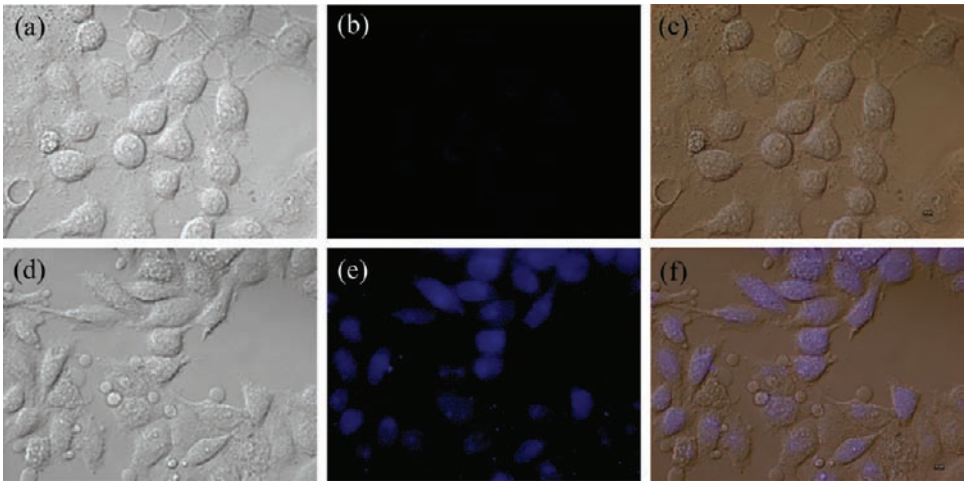

Figure 11. Fluorescence images of $\mathbf{L_2}$ with Zn^{2+} in HeLa cells (excitation at ~358 nm and emission at ~461 nm) in PBS buffer: (a) differential interference contrast microscopy (DIC) image of the HeLa cells treated with $\mathbf{L_2}$ (10 μM), PBS buffer pH 7.4; (b) fluorescence image of the same case as (a); (c) merged image of (a) and (b); (d) DIC microscopy image of the HeLa cells treated with $\mathbf{L_2}$ followed by 10 μM of Zn^{2+}/pyrithione (1/1) solution; (e) fluorescence image of the same case as (d); (f) merged image of (d) and (e). Each scale bar is 10 μm.

Intracellular Zn^{2+} Sensing by Fluorescence Microscopy. In order to demonstrate the utility of these amphiphilic calix[4]arene conjugates, viz., $\mathbf{L_1}$ and $\mathbf{L_2}$, in the recognition of Zn^{2+} in biological systems, HeLa cells were used as models (Experimental Section). HeLa cells were incubated in PBS buffer (pH 7.4) containing 10 μM of the conjugate ($\mathbf{L_1}$ or $\mathbf{L_2}$) for 20 min at 37 °C, followed by washing the cells with the same buffer to remove the excess of the conjugates. At this stage, the fluorescence microscopy image of HeLa cells displayed weak intracellular fluorescence. However, upon the addition of exogenous Zn^{2+} into the cells via incubation with $ZnSO_4$/pyrithione solution for 20 min at 37 °C, the cells exhibited highly intense blue fluorescence (Figure 11 and Supporting Information, Figure S20). Differential interference contrast microscopy (DIC) measurements for each experiment confirm that the cells are viable throughout the imaging experiments and the merged images support that the fluorescence is exhibited through the cells (Figure 11 and Supporting Information, Figure S20). The control experiments carried out with $ZnSO_4$/pyrithione solution alone do not show any fluorescence (Supporting Information, Figure S21).

Thus, HeLa cells incubated with $\mathbf{L_1}$ and $\mathbf{L_2}$ in the presence of Zn^{2+} showed much greater fluorescence emission as compared to the cells which were not incubated with this, suggesting that Zn^{2+} is responsible for enhancing the fluorescence of $\mathbf{L_1}$ and $\mathbf{L_2}$ in the cells, as it has also been shown to exhibit fluorescence enhancement in the solution medium (Figure 1). These results clearly indicate that the imino−phenolic−pyridyl conjugates of calix[4]arene, viz., $\mathbf{L_1}$ and $\mathbf{L_2}$, are effective intracellular Zn^{2+} imaging agents with cell permeability. To the best of our knowledge, this is the first known calix[4]arene-based conjugate in the literature which has been demonstrated to recognize Zn^{2+} in live cells.

Phosphate Recognition. Owing to the strong affinity of Zn^{2+} toward the phosphate, the highly fluorescent Zn^{2+} complexes $[Zn\mathbf{L_1}]$ and $[Zn\mathbf{L_2}]$ have been studied for their secondary sensing property toward phosphate-based anions.

Fluorescence Titration of $[Zn\mathbf{L_2}]$ with Anions. Isolated Zn^{2+} complexes of $\mathbf{L_1}$ and $\mathbf{L_2}$ show strong fluorescence emission at ~455 nm when excited at 390 nm. The secondary recognition capabilities of these complexes have been carried out by titrating them with different anions, viz., F^-, Cl^-, Br^-, I^-, N_3^-, CO_3^{2-}, NO_2^-, NO_3^-, SCN^-, SO_4^{2-}, ClO_4^-, HSO_4^-, HCO_3^-, $H_2PO_4^-$, and $P_2O_7^{4-}$ (PPi). The $[Zn\mathbf{L_1}]$, which is deprived of one methylene moiety in the arm as compared to $[Zn\mathbf{L_2}]$ (CH_2−Py vs CH_2−CH_2−Py), does not show any significant fluorescence change (Figure 12 and Supporting Information, Figure S22) toward any of these anion; however, $[Zn\mathbf{L_2}]$ shows quenching of fluorescence intensity in the case of almost all the phosphate ions. Thus, in the case of inorganic pyrophosphate (PPi), it shows maximum quenching and the sigmoidal plot exhibits saturation at ~1−2 equiv, as compared to all other inorganic phosphates studied, which show saturation at much higher equivalents, suggesting the strong chelating affinity of PPi toward Zn^{2+} (Figure 12). The fast and selective response of $[Zn\mathbf{L_2}]$ toward PPi as compared to many anions, including other phosphates, allows it to be a selective sensing molecular system for PPi.

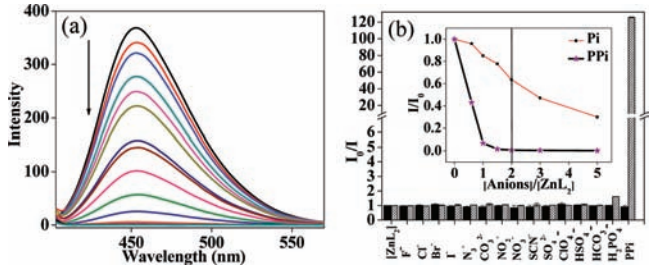

Figure 12. Fluorescence titration of $[Zn\mathbf{L_1}]$ and $[Zn\mathbf{L_2}]$ by different anions: (a) fluorescence spectra obtained during the titration of $[Zn\mathbf{L_2}]$ with PPi in aqueous methanolic (1/2 v/v) HEPES buffer (pH 7.4), with $[Zn\mathbf{L_2}]$ = 10 μM and λ_{ex} 390 nm; (b) relative fluorescence intensity (I_0/I) obtained during the titration of $[Zn\mathbf{L_1}]$ or $[Zn\mathbf{L_2}]$ with different anions (black bars are for $[Zn\mathbf{L_1}]$, and the bars with hatch lines are for $[Zn\mathbf{L_2}]$). The inset shows the relative fluorescence intensity (I/I_0) as a function of [anion]/$[Zn\mathbf{L_2}]$ mole ratio.

As $[Zn\mathbf{L_2}]$ has been found to recognize PPi among the 15 anions, the studies were extended to organic as well as biorelevant molecules bearing phosphate moiety, viz., β-naphthyl phosphate (NP) and adenosine mono-, di-, and triphosphates (AMP, ADP, and ATP). Among these, the

dx.doi.org/10.1021/ic202426v | Inorg. Chem. 2012, 51, 4994−5005

fluorescence quenching follows the order ATP > ADP ≫ AMP ≈ β-naphthyl phosphate, suggesting that the quenching is dependent both on the bulkiness of the organic moiety and on the number of phosphate moieties present (Figure 13). In order to assess the sensitivity of $[ZnL_2]$ for PPi sensing, fluorescence titrations were carried out between $[ZnL_2]$ vs [PPi] by keeping a 1/1 ratio. The results clearly demonstrate that $[ZnL_2]$ can detect up to 278 ± 10 ppb of PPi, suggesting that the detection limit is low enough to have some biological applications (Supporting Information, Figure S23).

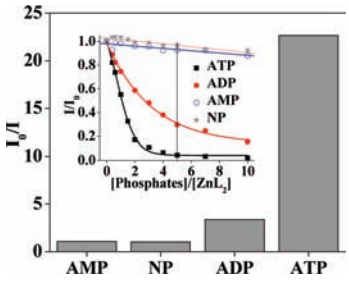

Figure 13. Relative fluorescence intensity (I_0/I) obtained during the titration of $[ZnL_2]$ with different organic phosphates in aqueous methanolic (1/2 v/v) HEPES buffer (pH 7.4), with $[ZnL_2]$ = 10 μM and λ_{ex} 390 nm. The inset shows a relative fluorescence intensity plot (I/I_0) for the titration of $[ZnL_2]$ with these pshosphates.

As $[ZnL_2]$ shows strong visual fluorescent color under UV light, experiments were carried out between $[ZnL_2]$ and different anions, including phosphate-bearing nucleotides, by keeping a 1/2 ($[ZnL_2]$/anion) mole ratio. The visual color changes from fluorescent to nonfluorescent in the presence of ATP and PPi, where the color is reminiscent of L_2. Thus, $[ZnL_2]$ clearly distinguishes biologically important ATP and PPi from a variety of other anions. The color changes thus observed in the fluorescence is attributable to the interaction with followed by the removal of Zn^{2+} from $[ZnL_2]$ by these anions. However, the color of $[ZnL_2]$ remains fluorescent in the presence of other anions, suggesting that Zn^{2+} is intact in the complex in the presence of these anions (Figure 14).

Absorption Titration of $[ZnL_2]$ with Anions. In order to support the results obtained from the fluorescence studies, similar titrations were carried out with absorption spectroscopy. Titration of $[ZnL_2]$ with PPi exhibits lowering of absorbance of the band at ~378 nm and further shows two new bands, one at ~325 nm and the other at ~420 nm, which correspond to the free receptor, and the absorbance of these bands increases (Figure 15). The absorbance vs mole ratio plot shows sigmoidal behavior, with saturation being acquired within ~1−2 equiv, similar to that observed from the fluorescence study (Figure 12).

The titrations carried out with other anions exhibited no significant change except in the case of ATP. The ADP and simple phosphates showed marginal changes in the absorption of the 377 nm band corresponding to $[ZnL_2]$. The absorption spectra obtained from the titration do not conform to the formation of free L_2 and hence are suggestive of the presence of intact $[ZnL_2]$ in the case of all the other anions (Figure 16).

^{1}H NMR Titrations. ^{1}H NMR titrations were carried out to check the removal of Zn^{2+} from $[ZnL_2]$ by polyphosphates. For this purpose ATP has been used instead of PPi because of the solubility and the precipitation problem faced in case of the use of Na_4(PPi) when taken in DMSO-d_6. During the titration of $[ZnL_2]$ with ATP, the signals corresponding to the complex start to disappear and the signals corresponding to free L_2 start to appear as the concentration of the added ATP increases and the signals of the complex completely disappeared at higher equivalents (Figure 17). and thus clearly supporting Zn^{2+} removal from its complex by releasing free L_2.

Reusability and Reversibility of the Receptor. The reusability of the calix[4]arene conjugate L_2 has been demonstrated by carrying out four alternative cycles of the titration of L_2 with Zn^{2+} followed by PPi. Zn^{2+} shows remarkable switch-on fluorescence changes through formation of $[ZnL_2]$, and further the titration (Supporting Information, Figure S24) of this fluorescent complex with PPi quenches the same by removing the Zn^{2+} from $[ZnL_2]$. The chemical reversibility behavior of the receptor with Zn^{2+}, followed by the removal of Zn^{2+} by PPi, was studied in HEPES buffered water−methanol solution. The switch-on and -off action of L_2 could be studied by monitoring the fluorescence changes as a function of the addition of Zn^{2+} followed by PPi, for four consecutive cycles, wherein remarkable reversal of the fluorescence intensity was observed (Figure 18). Hence, L_2 is a reversible and reusable sensor for Zn^{2+} and its zinc complex $[ZnL_2]$ as a secondary sensor for PPi.

■ CONCLUSIONS AND CORRELATIONS

The imino−phenolic−pyridyl conjugates of calix[4]arene L_1 and L_2 have been synthesized and characterized. These were found to be sensitive and selective receptors for Zn^{2+} in HEPES buffer medium. Their selectivity and sensitivity were demonstrated on the basis of fluorescence, absorption, and ^{1}H NMR spectroscopy, ESI mass spectrometry, and visual fluorescent color changes. L_1 and L_2 can detect Zn^{2+} up to ~31 and ~112 ppb, respectively by switch-on fluorescence, suggesting its applicability to detect Zn^{2+} ions in aqueous HEPES buffer medium. TDDFT calculations were carried out to demonstrate the electronic properties of L_1 and L_2 and their corresponding zinc complexes. The structure of $[ZnL_1]$ has been established by single-crystal XRD, and in this the zinc center shows a square-pyramidal geometry by using an N_3O_2 core formed by two phenolic oxygens, two imine nitrogens of both the arms, and one pyridyl nitrogen from one of the arms of the calix[4]arene unit. In the lattice, two water molecules were found which connect the two neighboring calix[4]arene units through hydrogen bonding, thereby resulting in the formation

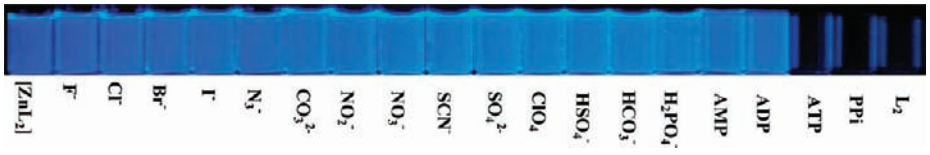

Figure 14. Vials showing the color changes observed when different anions were added to a solution of $[ZnL_2]$ in 2/1 mol ratio under (near-UV) 365 nm light.

dx.doi.org/10.1021/ic202426v | Inorg. Chem. 2012, 51, 4994−5005

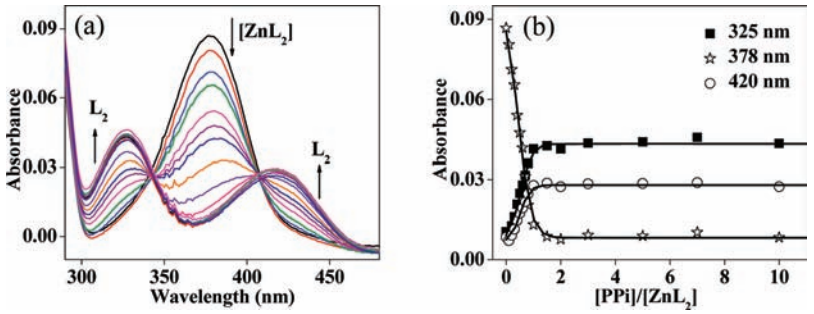

Figure 15. (a) Absorption spectra obtained during the titration of $[ZnL_2]$ with PPi in aqueous methanolic (1/2 v/v) HEPES buffer (pH 7.4). (b) Plot of absorbance vs $[PPi]/[ZnL_2]$ for different absorption bands.

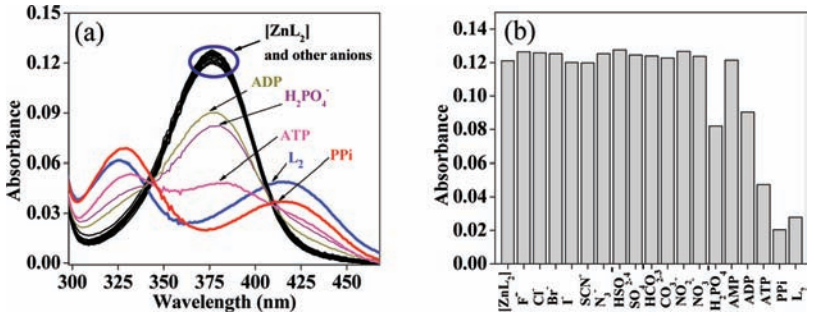

Figure 16. (a) Absorption spectra obtained during the titration of $[ZnL_2]$ with different anions in aqueous methanolic (1/2 v/v) HEPES buffer (pH 7.4). (b) Histogram showing the absorbance of $[ZnL_2]$ at the 377 nm band, on titration with different anions.

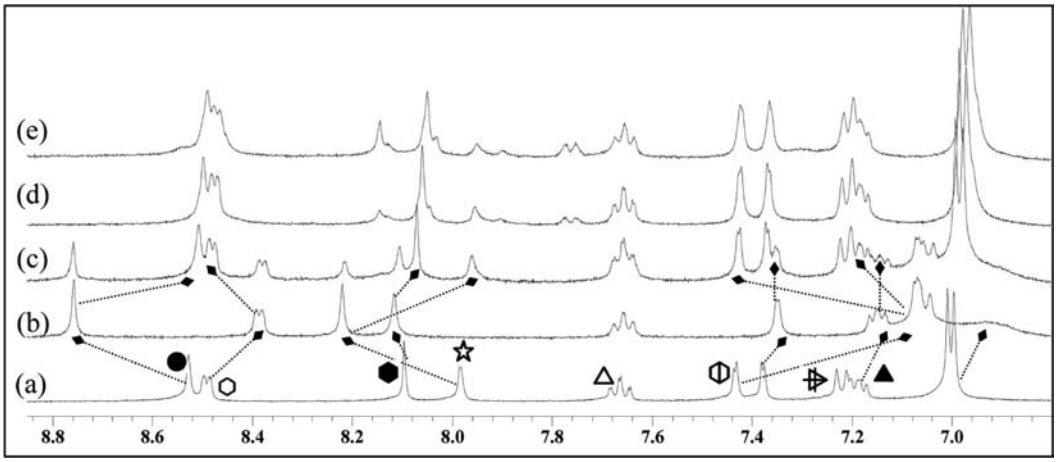

Figure 17. ^{1}H NMR spectral titration in a DMSO-d_6/D_2O mixture (2/1): (a) L_2; (b) $[ZnL_2]$; (c–e) $[ZnL_2]$ + n equivalents ATP (n = 1 (c), 2 (d), and 3 (e)). Legend to symbols: (●) imine-H; (⬡,▲, △, △ with bar) Py-H; (☆) calix-OH; (⬢) triazole-H; (⬡ with bar) Sal-H.

of dimers. The structure of $[ZnL_2]$ was computationally optimized using DFT calculations and found an almost similar type of zinc geometry, except that the Py-N···Zn distance is longer in the case of $[ZnL_2]$ as compared to that of $[ZnL_1]$. L_1 and L_2 were demonstrated as potential live-cell fluorescence imaging agents under microscopy using HeLa cells. Non-fluorescent images were observed when HeLa cells were incubated with these conjugates alone. However, strong fluorescence was observed in HeLa cells in the presence of Zn^{2+}. Hence, these results clearly indicate that the imino–phenolic–pyridyl conjugates of calix[4]arene, viz., L_1 and L_2, are effective intracellular Zn^{2+} imaging agents with cell permeability.

These fluorescent zinc complexes, viz., $[ZnL_1]$ and $[ZnL_2]$, have been subjected to studies of their secondary sensing properties toward various anions. The fluorescence intensity of $[ZnL_1]$ has been found to be unaltered in the presence of all 18 anions studied, thus indicating the nonavailable nature of Zn^{2+} in its complex. However, $[ZnL_2]$ was found to be selective toward phosphate-bearing ions and molecules and is sensitive as well as selective in particular to PPi and ATP among all the anions studied, including phosphates. The selectivity has been shown on the basis of fluorescence and absorption spectroscopy studies. $[ZnL_2]$ was able to detect a minimum concentration of PPi up to 278 ± 10 ppb at pH 7.4 in aqueous methanolic HEPES buffer. The unusual sensitivity and reactivity of $[ZnL_2]$ over $[ZnL_1]$ toward phosphates is attributable to a highly distorted geometry with long a Zn–N_{Py} bond found in the former.

dx.doi.org/10.1021/ic202426v | Inorg. Chem. 2012, 51, 4994–5005

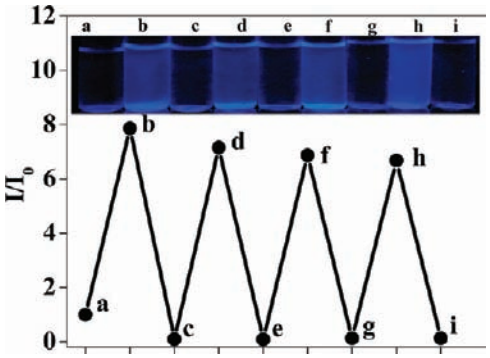

Figure 18. Fluorescence experiment to show the reversibility and reusability of the receptor for sensing Zn^{2+} and PPi by alternate addition of these two to $\mathbf{L_2}$: (bottom) relative fluorescence intensity (I/I_0) obtained during the titration of $\mathbf{L_2}$ with Zn^{2+} and PPi in aqueous methanolic (1/2 v/v) HEPES buffer (pH 7.4), with $[\mathbf{L_2}] = 10\ \mu M$ and λ_{ex} 390 nm; (top) visual fluorescent color change after each addition. Labels: (a) $\mathbf{L_2}$; (b) {(a) + Zn^{2+}}; (c) {(b) + PPi}; (d) {(c) + Zn^{2+}}; (e) {(d) + PPi}; (f) {(e) + Zn^{2+}}; (g) {(f) + PPi}; (h) {(g) + Zn^{2+}}; (i) {(h) + PPi}.

■ ASSOCIATED CONTENT

Ⓢ Supporting Information

Figures, text, tables, and a CIF file giving X-ray crystallographic data for $[Zn\mathbf{L_1}]$, synthesis and characterization details of precursor molecules, ^1H NMR, ^{13}C NMR, and mass spectral data for all calix[4]arene conjugates, XRD data of $[Zn\mathbf{L_1}]$, computational data for $[Zn\mathbf{L_2}]$, TDDFT data, and fluorescence and absorption spectra. This material is available free of charge via the Internet at http://pubs.acs.org.

■ AUTHOR INFORMATION

Corresponding Author

*Tel: 91 22 2576 7162. Fax: 91 22 2572 3480. E-mail: cprao@iitb.ac.in.

Notes

The authors declare no competing financial interest.

■ ACKNOWLEDGMENTS

C.P.R. acknowledges financial support by the DST, CSIR, and BRNS-DAE. D.P. acknowledges financial support by a DAE-SRC fellowship, Department of Atomic Energy, Government of India. R.K.P. and A.R. thank the CSIR for their Senior Research Fellowships.

■ REFERENCES

(1) (a) Dudev, T. *Chem. Rev.* **2003**, *103*, 773. (b) Lipscomb, W. N.; Strater, N. *Chem. Rev.* **1996**, *96*, 2375. (c) Jiang, P.; Guo, Z. *Coord. Chem. Rev.* **2004**, *248*, 205.

(2) (a) Frederickson, C. J.; Suh, S. W.; Koh, J.-Y.; Cha, Y. K.; Thompson, R. B.; LaBuda, C. J.; Balaji, R. V.; Cuajungco, M. P. *J. Histochem. Cytochem.* **2002**, *50*, 1659. (b) Danscher, G.; Stoltenberg, M. *J. Histochem. Cytochem.* **2005**, *53*, 141. (c) Chang, C. J.; Jaworski, J.; Nolan, E. M.; Sheng, M.; Lippard, S. J. *Proc. Natl. Acad. Sci. U.S.A.* **2004**, *101*, 1129.

(3) (a) Zalewski, P. D.; Millard, S. H.; Forbes, I. J.; Kapaniris, O.; Slavotinek, A.; Betts, W. H.; Ward, A. D.; Lincoln, S. F.; Mahadevan, I. *J. Histochem. Cytochem.* **1994**, *42*, 877. (b) Lukowiak, B.; Vandewalle, B.; Riachy, R.; Conte, J.-K.; Gmyr, V.; Belaich, S.; Lefebvre, J.; Pattou, F. *J. Histochem. Cytochem.* **2001**, *49*, 519.

(4) Sorensen, M. B.; Stoltenberg, M.; Juhl, S.; Danscher, G.; Ernst, E. *Prostate* **1997**, *31*, 125.

(5) (a) Cuajungco, M. P.; Lees, G. J. *Neurobiol. Dis.* **1997**, *4*, 137. (b) Bush, A. I.; Tanzi, R. E. *Proc. Natl. Acad. Sci. U.S.A.* **2002**, *99*, 7317. (c) Larson, A. A.; Kitto, K. F. *J. Pharmacol. Exp. Ther.* **1997**, *282*, 1319. (d) Hogstrand, C.; Kille, P.; Nicholson, R. I.; Taylor, K. M. *Trends Mol. Med.* **2009**, *15*, 101.

(6) (a) Eide, D. J. *Biochim. Biophys. Acta* **2006**, *1763*, 711. (b) Gunnlaugsson, T.; Glynn, M.; Gillian, M. T.; Kruger, P. E.; Pfeffer, F. M. *Coord. Chem. Rev.* **2006**, *250*, 3094.

(7) (a) Ronaghi, M.; Karamohamed, S.; Pettersson, B.; Uhlen, M.; Nyren, P. *Anal. Biochem.* **1996**, *242*, 84. (b) Kim, S. K.; Lee, D. H.; Hong, J.-N.; Yoon, J. *Acc. Chem. Res.* **2009**, *42*, 23. (c) Zyryanov, G. V.; Palacios, M. A.; Anzenbacher, P. *Angew. Chem., Int. Ed.* **2007**, *46*, 1. (d) Beer, P. D.; Gale, P. A. *Angew. Chem., Int. Ed.* **2001**, *40*, 486. (e) Fabbrizzi, L.; Licchelli, M.; Rabaioli, G.; Taglietti, A. *Coord. Chem. Rev.* **2000**, *205*, 85. (f) Lee, J. Y.; Hirose, M. *J. Biol. Inorg. Chem.* **1992**, *267*, 14753.

(8) Nussey, S.; Whitehead, S. *Endocrinology: An Integrated Approach*; BIOS Scientific Publishers: Oxford, U.K., 2001.

(9) (a) Mizukami, S.; Nagano, T.; Urano, Y.; Odani, A.; Kikuchi, K. *J. Am. Chem. Soc.* **2002**, *124*, 3920. (b) Fabbrizzi, L.; Marcotte, N.; Stomeo, F.; Taglietti, A. *Angew. Chem., Int. Ed.* **2002**, *41*, 3811. (c) Lee, D. H.; Im, J. H.; Son, S. U.; Chung, Y. K.; Hong, J. I. *J. Am. Chem. Soc.* **2003**, *125*, 7752. (d) Lee, H. N.; Xu, Z.; Kim, S. K.; Swamy, K. M. K.; Kim, Y.; Kim, S. J.; Yoon, J. *J. Am. Chem. Soc.* **2007**, *129*, 3828. (e) Lee, H. N.; Swamy, K. M. K.; Kim, S. K.; Kwon, J. Y.; Kim, Y.; Kim, S. J.; Yoon, Y. J.; Yoon, J. *Org. Lett.* **2007**, *9*, 243. (f) Lee, J. H.; Park, J.; Lah, M. S.; Chin, J.; Hong, J. I. *Org. Lett.* **2007**, *9*, 3729. (g) Shao, N.; Jin, J.; Wang, G.; Zhang, Y.; Yang, R.; Yuan, J. *Chem. Commun.* **2008**, 1127.

(10) (a) Diamond, D. *Chem. Soc. Rev.* **1996**, 15. (b) de Silva, A. P.; Gunaratne, H. Q. N.; Gunnlaugsson, T.; Huxley, A. J. M.; McCoy, C. P.; Rademacher, J. T.; Rice, T. E. *Chem. Rev.* **1997**, *97*, 1515. (c) Unob, F.; Asfari, Z.; Vicens, J. *Tetrahedron Lett.* **1998**, *39*, 295. (d) Valeur, B.; Leray, I. *Coord. Chem. Rev.* **2000**, *205*, 3. (e) Bagatin, I. A.; de Souza, E. S.; Ito, A. S.; Toma, H. E. *Inorg. Chem. Commun.* **2003**, *6*, 288. (f) Ozturk, G.; Akkaya, E. U. *Org. Lett.* **2004**, *6*, 241. (g) Kim, S. K.; Lee, S. H.; Lee, J. Y.; Bartsch, R. A.; Kim, J. S. *J. Am. Chem. Soc.* **2004**, *126*, 16499. (h) Lee, J. Y.; Kim, S. K.; Jung, J. H.; Kim, J. S. *J. Org. Chem.* **2005**, *70*, 1463. (i) Khatua, S.; Choi, S. H.; Lee, J.; Kim, K.; Do, Y.; Churchill, D. G. *Inorg. Chem.* **2009**, *48*, 2993. (j) Kim, K.; Ha, Y.; Kaufman, L.; Churchill, D. G. *Inorg. Chem.* **2012**, *51*, 928.

(11) (a) Bakirci, H.; Koner, A. L.; Dickman, M. H.; Kortz, U.; Nau, W. M. *Angew. Chem., Int. Ed.* **2006**, *45*, 7400. (b) Kolusheva, S.; Zadmard, R.; Schrader, T.; Jelinek, R. *J. Am. Chem. Soc.* **2006**, *128*, 13592. (c) Lankshear, M. D.; Cowley, A. R.; Beer, P. D. *Chem. Commun.* **2006**, 612. (d) Gale, P. A.; Quesada, R. *Coord. Chem. Rev.* **2006**, *250*, 3219. (e) Quinlan, E.; Matthews, S. E.; Gunnlaugsson, T. *Tetrahedron Lett.* **2006**, *47*, 9333. (f) Lee, S. H.; Kim, H. J.; Lee, Y. O.; Vicens, J.; Kim, J. S. *Tetrahedron Lett.* **2006**, *47*, 4373. (g) Chang, K.-C.; Su, I.-H.; Lee, G.-H.; Chung, W.-S. *Tetrahedron Lett.* **2007**, *48*, 7274. (h) Chang, K.-C.; Su, I.-H.; Senthilvelan, A.; Chung, W.-S. *Org. Lett.* **2007**, *9*, 3363. (i) Kim, J. S.; Quang, D. T. *Chem. Rev.* **2007**, *107*, 3780. (j) Chaumet-Riffaud, P.; Martinez-Duncker, I.; Marty, A.-L.; Richard, C.; Prigent, A.; Moati, F.; Sarda-Mantel, L.; Scherman, D.; Bessodes, M.; Mignet, N. *Bioconjugate Chem.* **2010**, *21*, 589.

(12) (a) Quinlan, E.; Matthews, S. E.; Gunnlaugsson, T. *J. Org. Chem.* **2007**, *72*, 7497. (b) Park, S. Y.; Yoon, J. H.; Hong, C. S.; Souane, R.; Kim, J. S.; Matthews, S. E.; Vicens, J. *J. Org. Chem.* **2008**, *73*, 8212. (c) Filby, M. H.; Dickson, S. J.; Zaccheroni, N.; Prodi, L.; Bonacchi, S.; Montalti, M.; Paterson, M. J.; Humphries, T. D.; Chiorboli, C.; Steed, J. W. *J. Am. Chem. Soc.* **2008**, *130*, 4105. (d) Li, G.-K.; Xu, Z.-X.; Chen, C.-F.; Huang, Z.-T. *Chem. Commun.* **2008**, 1774. (e) Lankshear, M. D.; Dudley, I. M.; Chan, K.-M.; Cowley, A. R.; Santos, S. M.; Felix, V.; Beer, P. D. *Chem. Eur. J.* **2008**, *14*, 2248. (f) Lalor, R.; Baillie-Johnson, H.; Redshaw, C.; Matthews, S. E.; Mueller, A. *J. Am. Chem. Soc.* **2008**, *130*, 2892. (g) Senthilvelan, A.; Ho, I.-T.; Chang, K.-C.; Lee, G.-H.; Liu, Y.-H.; Chung, W.-S. *Chem. Eur. J.* **2009**, *15*, 6152. (h) Leray, I.; Valeur, B. *Eur. J. Inorg. Chem.* **2009**, 3525.

(13) (a) Kim, J. S.; Lee, S. Y.; Yoon, J.; Vicens, J. *Chem. Commun.* **2009**, 4791. (b) Creaven, B. S.; Donlon, D. S.; McGinley, J. *Coord.*

Chem. Rev. **2009**, *253*, 893. (c) Chang, K.-C.; Su, I.-H.; Wang, Y.-Y.; Chung, W.-S. *Eur. J. Org. Chem.* **2010**, 4700. (d) Xu, Z.; Yoon, J.; Spring, D. R. *Chem. Soc. Rev.* **2010**, *39*, 1996. (e) Zhang, J. F.; Bhuniya, S.; Lee, Y. H.; Bae, C.; Lee, J. H.; Kim, J. S. *Tetrahedron Lett.* **2010**, *51*, 3719. (f) Kumar, M.; Kumar, R.; Bhalla, V. *Org. Lett.* **2011**, *13*, 366. (g) He, X.; Yam, W. W. *Org. Lett.* **2011**, *13*, 2172. (h) Ni, X.-L.; Wang, S.; Zeng, X.; Tao, Z.; Yamato, T. *Org. Lett.* **2011**, *13*, 552. (i) McGinley, J.; Walsh, J. M. D. *Inorg. Chem. Commun.* **2011**, *14*, 1018. (j) Ni, X.-L.; Zeng, X.; Redshaw, C.; Yamato, T. *J. Org. Chem.* **2011**, *76*, 5696. (k) Sahin, O.; Yilmaz, M. *Tetrahedron* **2011**, *67*, 3501.

(14) (a) Dessingou, J.; Joseph, R.; Rao, C. P. *Tetrahedron Lett.* **2005**, *46*, 7967. (b) Joseph, R.; Ramanujam, B.; Acharya, A.; Khutia, A.; Rao, C. P. *J. Org. Chem.* **2008**, *73*, 5745. (c) Chinta, J. P.; Acharya, A.; Kumar, A.; Rao, C. P. *J. Phys. Chem. B* **2009**, *113*, 12075. (d) Joseph, R.; Ramanujam, B.; Acharya, A.; Rao, C. P. *J. Org. Chem.* **2009**, *74*, 8181. (e) Pathak, R. K.; Ibrahim, S. M.; Rao, C. P. *Tetrahedron Lett.* **2009**, *50*, 2730. (f) Joseph, R.; Chinta, J. P.; Rao, C. P. *J. Org. Chem.* **2010**, *75*, 3387. (g) Pathak, R. K.; Dikundwar, A. G.; Guru Row, T. N.; Rao, C. P. *Chem. Commun.* **2010**, *46*, 4345. (h) Acharya, A.; Ramanujam, B.; Chinta, J. P.; Rao, C. P. *J. Org. Chem.* **2011**, *76*, 127. (i) Joseph, R.; Chinta, J. P.; Rao, C. P. *Inorg. Chem.* **2011**, *50*, 7050. (j) Joseph, R.; Rao, C. P. *Chem. Rev.* **2011**, *111*, 4658. (k) Bandela, A.; Chinta, J. P.; Hinge, V. K.; Dikundwar, A. G.; Guru Row, T. N.; Rao, C. P. *J. Org. Chem.* **2011**, *76*, 1742.

(15) Frisch, M. J.; Trucks, G. W.; Schlegel, H. B.; Scuseria, G. E.; Robb, M. A.; Cheeseman, J. R.; Montgomery, J. A., Jr.; Vreven, T.; Kudin, K. N.; Burant, J. C.; Millam, J. M.; Iyengar, S. S.; Tomasi, J.; Barone, V.; Mennucci, B.; Cossi, M.; Scalmani, G.; Rega, N.; Petersson, G. A.; Nakatsuji, H.; Hada, M.; Ehara, M.; Toyota, K.; Fukuda, R.; Hasegawa, J.; Ishida, M.; Nakajima, T.; Honda, Y.; Kitao, O.; Nakai, H.; Klene, M.; Li, X.; Knox, J. E.; Hratchian, H. P.; Cross, J. B.; Adamo, C.; Jaramillo, J.; Gomperts, R.; Stratmann, R. E.; Yazyev, O.; Austin, A. J.; Cammi, R.; Pomelli, C.; Ochterski, J. W.; Ayala, P. Y.; Morokuma, K.; Voth, G. A.; Salvador, P.; Dannenberg, J. J.; Zakrzewski, V. G.; Dapprich, S.; Daniels, A. D.; Strain, M. C.; Farkas, O.; Malick, D. K.; Rabuck, A. D.; Raghavachari, K.; Foresman, J. B.; Ortiz, J. V.; Cui, Q.; Baboul, A. G.; Clifford, S.; Cioslowski, J.; Stefanov, B. B.; Liu, G.; Liashenko, A.; Piskorz, P.; Komaromi, I.; Martin, R. L.; Fox, D. J.; Keith, T.; Al-Laham, M. A.; Peng, C. Y.; Nanayakkara, A.; Challacombe, M.; Gill, P. M. W.; Johnson, B.; Chen, W.; Wong, M. W.; Gonzalez, C.; Pople, J. A. *Gaussian 03, revision C.02*; Gaussian, Inc., Wallingford, CT, 2004.

(16) (a) Mameli, M.; Aragoni, M.; Arca, M.; Caltagirone, C.; Demartin, F.; Farruggia, G.; De Filippo, G.; Devillanova, F.; Garau, A.; Isaia, F.; Lippolis, V.; Murgia, S.; Prodi, L.; Pintus, A.; Zaccheroni, N. *Chem. Eur. J.* **2010**, *16*, 919. (b) Jung, H. S.; Ko, K. C.; Lee, J. H.; Kim, S. H.; Bhuniya, S.; Lee, J. Y.; Kim, Y.; Kim, S. J.; Kim, J. S. *Inorg. Chem.* **2010**, *49*, 8552. (c) Ko, C. K.; Wu, J. -S.; Kim, H. J.; Kwon., P. S.; Kim, J. W.; Bartsch, R. A.; Lee, J. Y.; Kim, J. S. *Chem. Commun.* **2011**, *47*, 3165.

(17) (a) Lambert, E.; Chabut, B.; Chardon-Noblat, S.; Deronzier, A.; Chottard, G.; Bousseksou, A.; Tuchagues, J.-P.; Laugier, J.; Bardet, M.; Latour, J.-M. *J. Am. Chem. Soc.* **1997**, *119*, 9424. (b) Shao, N.; Zhang, Y.; Cheung, S.; Yang, R.; Chan, W.; Mo, T.; Li, K.; Liu, F. *Anal. Chem.* **2005**, *77*, 7294. (c) Wang, Q.; Wilson, C.; Blake, A. J.; Collinson, S. R.; Tasker, P. A.; Schroder, M. *Tetrahedron Lett.* **2006**, *47*, 8983.

(18) (a) Zhao, J.; Zhao, B.; Liu, J.; Ren, A.; Feng, J. *Chem. Lett.* **2006**, 268. (b) Wang, L.; Qin, W.; Tang, X.; Dou, W.; Liu, W. *J. Phys. Chem. A* **2011**, *115*, 1609. (c) Gorner, H.; Khanra, S.; Weyhermuller, T.; Chaudhari, P. *J. Phys. Chem. A* **2006**, *110*, 2587. (d) Wang, L.; Qin, W.; Liu, W. *Inorg. Chem. Commun.* **2010**, *13*, 1122. (e) Wu, J.; Liu, W.; Ge, J.; Zhang, H.; Wang, P. *Chem. Soc. Rev.* **2011**, *40*, 3483.